Numerical resolution of an electromagnetic inverse medium problem at fixed frequency

Maya de Buhan[1,*]

[1] *CNRS, UMR 8145, MAP5, Université Paris Descartes, Sorbonne Paris Cité, France;*

Marion Darbas[2,†]

[2] *CNRS UMR 7352, LAMFA, Université de Picardie Jules Verne, Amiens, France;*

September 26, 2016

Abstract

The aim of this paper is to solve numerically the inverse problem of determining the complex refractive index of an electromagnetic medium from partial boundary field measurements at a fixed frequency. The governing equations are the time-harmonic Maxwell equations formulated in electric field in a two-dimensional bounded domain. We express the inverse problem as the minimization of a cost function representing the difference between the measured and predicted fields. Our numerical reconstruction algorithm combines the BFGS method and an iterative process, called the Adaptive Eigenspace Inversion. The unknown complex coefficient is expanded in terms of eigenfunctions of an elliptic operator. Both the eigenspace and the mesh are iteratively adapted during the minimization procedure. Numerical experiments illustrate the performance of the reconstruction for various configurations.

Keywords: Inverse medium problem, Maxwell's equations, cost functional, minimization iterative process, Adaptive Eigenspace Method, numerical reconstruction.

1 Introduction

The present paper deals with the numerical resolution of an electromagnetic inverse medium problem. More precisely, we consider the problem of determining the complex refractive index of a medium, namely the dielectric permittivity (real part) and the electric conductivity (imaginary part), from a finite number of boundary field measurements at a fixed frequency. The governing equations are the time-harmonic Maxwell equations formulated in electric field in a two-dimensional bounded domain. Such an electromagnetic inverse problem arises in various areas of science and engineering with many applications, e.g. in medical imaging, geophysical exploration or non-destructive testing. For instance, microwave imaging (electromagnetic high frequencies) is under investigation for cancer screening or brain stroke detection (see Tournier *et al* [30, 31]). Numerical methods that are able to highlight dielectric contrast between normal and possibly abnormal tissue are of interest.

From a mathematical point of view, the considered inverse medium problem is severely ill-posed and we refer the reader to the book [29] by Romanov and Kabanikhin. Indeed, coefficients of elliptic problems (like the time-harmonic Maxwell problem) in a bounded domain are uniquely

*e-mail: maya.de-buhan@parisdescartes.fr

†e-mail: marion.darbas@u-picardie.fr

determined by the entire Dirichlet-to-Neumann map on the whole boundary of the domain (e.g. Ola, Païvärinta and Somersalo [25], Caro, Ola and Salo [12], Kenig, Salo and Uhlman [23] and references therein). A typical problem of this type is Calderón's inverse conductivity problem [11]. Nevertheless, it is legitimate to search for reconstruction methods using partial information on the Dirichlet-to-Neumann map, which is often the case in practice. Several analytical and numerical studies have been devoted to the detection of inhomogeneities in the electromagnetic parameters of a body. Ammari *et al* (e.g. [2, 3]) have introduced asymptotic methods to reconstruct small amplitude perturbations in coefficients from measurements on a part of the boundary. This yields constructive numerical methods for the localization of electromagnetic defects (e.g. Ammari *et al* [1], Asch and Mefire [4], Darbas and Lohrengel [15]). Concerning minimization approaches, Beilina *et al* (e.g. [7, 8]) have developed an adaptive finite element method based on a posteriori estimates. Other successful methods have been proposed in the literature for the numerical solution of the electromagnetic scattering medium problem. Data are in this case measurements of the far-field pattern of the scattered field. Without being exhaustive, we can mention among them the linear sampling method of Haddar and Monk [20], a preconditioned Newton method initiated by Hohage [22], or a regularized recursive linearization method used by Bao and Li [5].

Here, we propose to formulate the inverse medium problem as the minimization of a cost function representing the difference between the measured and predicted fields. To solve the minimization problem, we use a gradient-based quasi-Newton algorithm. The main goal of this paper is to present a reconstruction method for the unknown complex refractive index of the medium from boundary measurements. The idea is to project it into a basis composed by eigenvectors of the Laplacian operator. Then, the method uses an iterative process to adapt the mesh and the basis of eigenfunctions to the previous approximation during the minimization procedure. This method is called *Adaptive Eigenspace Inversion*. We compare it with a more standard choice given by a linear piecewise approximation of the coefficients. The Adaptive Eigenspace Inversion (AEI or referred sometimes as AI) method has been initially proposed for the viscoelastic system by de Buhan and Osses [9]. Then, it has been successfully applied to an inverse scattering problem for the wave equation in a paper of de Buhan and Kray [10]. In both cases, time evolution problems of hyperbolic type are treated. The geometric optics condition of Bardos-Lebeau-Rauch [6], which allows that the associated inverse problems are uniquely solved, is satisfied. More precisely, the part of the boundary where the measurements (namely the normal derivative of the solution) are recorded, and the final observation time control geometrically the domain in the sense of [6]. The application of the AEI method to time-harmonic problems is a new area of research. This is the aim of the present work in electromagnetics, and also the one of Grote, Kray and Nahum which study the resolution of an inverse problem for the Helmholtz equation. In [18, 19], they proposed to combine a new AEI method and a frequency stepping process where the frequency of the incident field is iteratively increasing, with successful results. In the inverse problem we consider in this paper, we restrict ourselves to a fixed frequency. This is motivated by biomedical applications that we have in mind [30, 31]. Biological tissues are dispersive [17], that is to say their dielectric properties are frequency-dependent. We are not interested in finding this dependency law but only in discriminating between healthy and abnormal tissues. This can be achieved with a single frequency and changing the frequency does not provide more information.

The remainder of the paper is organized as follows. In Section 2 we present the forward problem under consideration. The formulation of the inverse problem is addressed in Section 3. It is formulated as a nonlinear optimization problem. The key-point is the evaluation of the gradient of the cost function where we use the adjoint method. In Section 4 we describe the reconstruction method based on the AEI method from a methodological point of view. Then, in Section 5, various numerical results are reported to discuss the advantages and limits of the method. Finally, we give some concluding remarks.

2 The forward problem

Let Ω be a bounded domain in $\mathbb{R}^2$ with a smooth boundary $\Gamma := \partial\Omega$. We denote by μ_0 and ε_0 the permeability and the permittivity of the vacuum. We assume that Ω is filled with a non-magnetic (i.e. constant permeability $\mu = \mu_0$) and isotropic medium of dielectric permittivity $\varepsilon = \varepsilon(\mathbf{x})$ and electrical conductivity $\sigma = \sigma(\mathbf{x})$, $\mathbf{x} \in \Omega$. We consider the system of 2D Maxwell equations

$$\nabla \times \boldsymbol{\mathcal{E}} = -\partial_t \mathcal{B}, \qquad \boldsymbol{\nabla} \times \mathcal{H} = \partial_t \boldsymbol{\mathcal{D}} + \boldsymbol{\mathcal{J}}, \text{ in } \Omega, \tag{2.1}$$

where $(\boldsymbol{\mathcal{E}}, \mathcal{H})$ are the electric and magnetic fields, $(\mathcal{B}, \boldsymbol{\mathcal{D}})$ are the magnetic and electric flux densities and $\boldsymbol{\mathcal{J}}$ represents the electrical current density. Notice that in two dimensions, the vector rotational operator is defined for a scalar function φ by $\boldsymbol{\nabla} \times \varphi = (\partial_2\varphi, -\partial_1\varphi)^t$, whereas the scalar rotational operator acting on a vector field $\mathbf{v} = (v_1, v_2)$ is given by $\nabla \times \mathbf{v} = \partial_1 v_2 - \partial_2 v_1$. We assume linear and isotropic constitutive relations

$$\mathcal{B} = \mu_0 \mathcal{H}, \quad \boldsymbol{\mathcal{D}} = \varepsilon \boldsymbol{\mathcal{E}}, \text{ and } \boldsymbol{\mathcal{J}} = \sigma \boldsymbol{\mathcal{E}}. \tag{2.2}$$

The wave equation for the electric field with no source term can be derived from (2.1) and (2.2) by eliminating the magnetic field as

$$\boldsymbol{\nabla} \times (\nabla \times \boldsymbol{\mathcal{E}}) + \mu_0(\varepsilon \partial_t^2 \boldsymbol{\mathcal{E}} + \sigma \partial_t \boldsymbol{\mathcal{E}}) = 0.$$

Considering the harmonic dependence in time of the form $\mathcal{E}(t, \mathbf{x}) = \Re(e^{-i\omega t}\mathbf{E}(\mathbf{x}))$, the electric field $\mathbf{E}$ satisfies the following equation in the frequency domain

$$\boldsymbol{\nabla} \times (\nabla \times \mathbf{E}) - k^2 \kappa \mathbf{E} = \mathbf{0}, \text{ in } \Omega, \tag{2.3}$$

where $k = \omega\sqrt{\varepsilon_0\mu_0}$ is the wavenumber and the function

$$\kappa(\mathbf{x}) = \frac{1}{\varepsilon_0}\big(\varepsilon(\mathbf{x}) + i\frac{\sigma(\mathbf{x})}{\omega}\big), \ \mathbf{x} \in \Omega, \tag{2.4}$$

is the refractive index of the medium. We assume $\varepsilon, \sigma \in L^\infty(\Omega)$ and that there are constants $\underline{\varepsilon}, \overline{\varepsilon} > 0$, $\underline{\sigma}, \overline{\sigma} > 0$ such that $\underline{\varepsilon} \le \varepsilon(\mathbf{x}) \le \overline{\varepsilon}$ and $\underline{\sigma} \le \sigma(\mathbf{x}) \le \overline{\sigma}$ a.e. in Ω. Let $\mathbf{n} = (n_1, n_2)^t$ denote the outward unit normal to Γ. We impose the boundary condition

$$(\nabla \times \mathbf{E}) \times \mathbf{n} = \mathbf{g}, \quad \text{on } \Gamma. \tag{2.5}$$

For a scalar function φ, we have $\varphi \times \mathbf{n} = (-\varphi n_2, \varphi n_1)^t$. We denote by $\mathbf{E}[\kappa]$ the solution of (2.3)-(2.5) associated with the refractive index κ. Existence and uniqueness results on the boundary-value problem (2.3)-(2.5) can be found in [14, 26]. We introduce the following functional space

$$H(\mathrm{curl}; \Omega) = \{\mathbf{E} \in L^2(\Omega)^2 | \nabla \times \mathbf{E} \in L^2(\Omega)\}.$$

Assume that $\mathbf{g} \in L^2(\Gamma)^2$, the variational formulation of the problem (2.3)-(2.5) is given by

$$\begin{cases} \text{Find } \mathbf{E} \in H(\mathrm{curl}; \Omega) \text{ such that} \\ \displaystyle\int_\Omega \big[(\nabla \times \mathbf{E})(\nabla \times \boldsymbol{\psi}) - k^2\kappa \mathbf{E} \cdot \boldsymbol{\psi}\big]\, d\mathbf{x} = \int_\Gamma \mathbf{g} \cdot \boldsymbol{\psi} ds, \qquad \forall \boldsymbol{\psi} \in H(\mathrm{curl}; \Omega). \end{cases} \tag{2.6}$$

Discretization and numerical solution of the forward problem will be mentioned in Section 5.

3 Formulation of the inverse problem

The inverse medium problem that interests us reads

$$(\mathcal{P}) \qquad \left\{ \begin{array}{l} \text{Given a frequency } \omega > 0, \\ \text{reconstruct the exact coefficient } \kappa_{ex}(\mathbf{x}),\ \mathbf{x} \in \Omega, \text{ defined by (2.4)}, \\ \text{from the boundary measurement } \mathbf{E}_{\rm obs} := \mathbf{E}[\kappa_{ex}] \text{ on } \Gamma_0, \end{array} \right.$$

where Γ_0 is a part of the boundary Γ including the case $\Gamma_0 = \Gamma$. Consequently, we recover the dielectric permittivity $\varepsilon(\mathbf{x})$ and the electrical conductivity $\sigma(\mathbf{x})$, $\mathbf{x} \in \Omega$, of the medium. We formulate the inverse problem as a minimization problem. We solve it using the Broyden-Fletcher-Goldfarb-Shanno (BFGS) algorithm [27]. This method of quasi-Newton type requires the computation of the gradient of the cost function with respect to the parameter at each iteration. The gradient is efficiently evaluated using the adjoint method.

3.1 A minimization problem

Problem $(\mathcal{P})$ is written as an optimization problem, namely it is replaced by the minimization of the following functional

$$J(\kappa) = \frac{1}{2} \int_{\Gamma_0} |(\mathbf{E}[\kappa] - \mathbf{E}_{\rm obs}) \times \mathbf{n}|^2 ds, \tag{3.1}$$

where $\mathbf{E}[\kappa]_{|\Gamma_0}$ is computed by solving the forward problem (2.3)-(2.5) at a fixed frequency $\omega > 0$ for a given refractive index κ and a boundary data $\mathbf{g}$, and $\mathbf{E}_{{\rm obs}|\Gamma_0}$ is the measured electric field. The functional J represents the error between the observed electric field and that predicted by Maxwell equations. The minimization problem

$$\min_{\kappa \in L^\infty(\Omega)} J(\kappa) \tag{3.2}$$

is solved by using the BFGS algorithm. The Hessian of the cost function J is approximated by means of the gradient of J. The functional and its gradient have to be computed within each iteration step.

3.2 Computation of the gradient using the adjoint method

In this section, we derive an expression of the derivative of the cost function J with respect to the coefficient κ in a given arbitrary direction $\delta\kappa$. The directional derivative of J is defined by

$$D_\kappa J(\kappa)\delta\kappa = \lim_{t \to 0} \frac{J(\kappa + t\delta\kappa) - J(\kappa)}{t}.$$

We introduce $\delta\mathbf{E} := \delta\mathbf{E}[\kappa, \delta\kappa]$ the solution of the following linearized problem

$$\left\{ \begin{array}{ll} \boldsymbol{\nabla} \times (\nabla \times \delta\mathbf{E}) - k^2 \kappa \delta\mathbf{E} = k^2 \delta\kappa \mathbf{E}[\kappa], & \text{in } \Omega, \\ (\nabla \times \delta\mathbf{E}) \times \mathbf{n} = 0, & \text{on } \Gamma. \end{array} \right. \tag{3.3}$$

We have $\mathbf{E}[\kappa + t\delta\kappa] = \mathbf{E}[\kappa] + t\delta\mathbf{E} + o(t^2)$. We obtain

$$\begin{array}{rcl} D_\kappa J(\kappa)\delta\kappa & = & \displaystyle \lim_{t \to 0} \frac{1}{2t} \left[\int_{\Gamma_0} (|(\mathbf{E}[\kappa + t\delta\kappa] - \mathbf{E}_{\rm obs}) \times \mathbf{n}|^2 - |(\mathbf{E}[\kappa] - \mathbf{E}_{\rm obs}) \times \mathbf{n}|^2) ds \right] \\ & = & \displaystyle \lim_{t \to 0} \frac{1}{t} \left[\int_{\Gamma_0} t \Re\Big((\overline{(\mathbf{E}[\kappa] - \mathbf{E}_{\rm obs}) \times \mathbf{n}})(\delta\mathbf{E} \times \mathbf{n}) \Big) ds + \frac{1}{2} \int_{\Gamma_0} t^2 |\delta\mathbf{E} \times \mathbf{n}|^2 ds \right] \\ & = & \displaystyle \Re\Big(\int_{\Gamma_0} (\overline{(\mathbf{E}[\kappa] - \mathbf{E}_{\rm obs}) \times \mathbf{n}})(\delta\mathbf{E} \times \mathbf{n}) ds \Big). \end{array} \tag{3.4}$$

The adjoint state method allows to simplify this expression. Let $\mathbf{F}$ be a test function. The variational formulation of the linearized equation (3.3) is given by

$$k^2 \int_\Omega \delta\kappa \mathbf{E}[\kappa] \cdot \overline{\mathbf{F}} d\mathbf{x} = \int_\Omega \big(\boldsymbol{\nabla} \times (\nabla \times \delta\mathbf{E}) - k^2 \kappa \delta\mathbf{E}\big) \cdot \overline{\mathbf{F}}\, d\mathbf{x}.$$

By integrating by parts the right-hand side of the previous formulation and using the boundary conditions satisfied by $\delta\mathbf{E}$, we obtain

$$\begin{aligned} k^2 \int_\Omega \delta\kappa \mathbf{E}[\kappa] \cdot \overline{\mathbf{F}} d\mathbf{x} &= \int_\Omega \big(\boldsymbol{\nabla} \times (\nabla \times \overline{\mathbf{F}}) - k^2 \kappa \overline{\mathbf{F}}\big) \cdot \delta\mathbf{E} d\mathbf{x} \\ &\quad - \int_\Gamma ((\nabla \times \delta\mathbf{E}) \times \mathbf{n}) \cdot \overline{\mathbf{F}}\, ds + \int_\Gamma ((\nabla \times \overline{\mathbf{F}}) \times \mathbf{n}) \cdot \delta\mathbf{E}\, ds \\ &= \int_\Omega \big(\boldsymbol{\nabla} \times (\nabla \times \overline{\mathbf{F}}) - k^2 \kappa \overline{\mathbf{F}}\big) \cdot \delta\mathbf{E} d\mathbf{x} + \int_\Gamma ((\nabla \times \overline{\mathbf{F}}) \times \mathbf{n}) \cdot \delta\mathbf{E}\, ds. \end{aligned}$$

Next, we choose $\overline{\mathbf{F}} := \overline{\mathbf{F}}[\kappa]$ the adjoint variable of $\delta\mathbf{E}$ satisfying

$$\boldsymbol{\nabla} \times (\nabla \times \overline{\mathbf{F}}) - k^2 \kappa \overline{\mathbf{F}} = 0, \text{ in } \Omega, \tag{3.5}$$

with the boundary condition

$$(\nabla \times \overline{\mathbf{F}}) \times \mathbf{n} = \begin{cases} \overline{((\mathbf{E}[\kappa] - \mathbf{E}_{obs}) \times \mathbf{n})} \times \mathbf{n}, & \text{on } \Gamma_0, \\ \mathbf{0}, & \text{on } \Gamma \setminus \Gamma_0. \end{cases} \tag{3.6}$$

We get

$$k^2 \int_\Omega \delta\kappa \mathbf{E}[\kappa] \cdot \overline{\mathbf{F}}[\kappa] d\mathbf{x} = - \int_{\Gamma_0} \overline{((\mathbf{E}[\kappa] - \mathbf{E}_{obs}) \times \mathbf{n})} (\delta\mathbf{E} \times \mathbf{n}) d\mathbf{x}.$$

Consequently, the differential (3.4) of the functional J is given by

$$D_\kappa J(\kappa)\delta\kappa = -k^2 \Re\Big(\int_\Omega \delta\kappa \mathbf{E}[\kappa] \cdot \overline{\mathbf{F}}[\kappa] d\mathbf{x} \Big). \tag{3.7}$$

At each step of the algorithm, the computation of the gradient needs to solve the forward problem (2.3)-(2.5) and the associated adjoint problem (3.5)-(3.6) for the coefficient κ in order to obtain the variables $\mathbf{E}$ and $\mathbf{F}$ respectively.

In practice, we perform multiple observations $\mathbf{E}^j_{\text{obs}}$, $1 \le j \le M$, of the electric field on Γ_0 at a fixed frequency ω. Each measurement $\mathbf{E}^j_{\text{obs}}$ is associated with the boundary data $\mathbf{g}^j$. Then, we can simply define the functional

$$J^M(\kappa) = \frac{1}{2} \sum_{j=1}^{M} \int_{\Gamma_0} |(\mathbf{E}^j[\kappa] - \mathbf{E}^j_{\text{obs}}) \times \mathbf{n}|^2 ds, \tag{3.8}$$

where the electric field $\mathbf{E}^j$ is solution to the problem

$$\begin{cases} \boldsymbol{\nabla} \times (\nabla \times \mathbf{E}^j) - k^2 \kappa \mathbf{E}^j = \mathbf{0}, & \text{in } \Omega, \\ (\nabla \times \mathbf{E}^j) \times \mathbf{n} = \mathbf{g}^j, & \text{on } \Gamma. \end{cases} \tag{3.9}$$

We have the following expression of the gradient in the direction $\delta\kappa$

$$D_\kappa J^M(\kappa)\delta\kappa = -k^2 \sum_{j=1}^{M} \Re \left[\int_\Omega \delta\kappa \mathbf{E}^j[\kappa] \cdot \overline{\mathbf{F}^j}[\kappa] d\mathbf{x} \right], \tag{3.10}$$

with $\overline{\mathbf{F}^j}$ satisfying the adjoint problem

$$\begin{cases} \boldsymbol{\nabla} \times (\nabla \times \overline{\mathbf{F}^j}) - k^2 \kappa \overline{\mathbf{F}^j} = \mathbf{0}, & \text{in } \Omega, \\ (\nabla \times \overline{\mathbf{F}^j}) \times \mathbf{n} = \overline{((\mathbf{E}^j[\kappa] - \mathbf{E}^j_{\text{obs}}) \times \mathbf{n})} \times \mathbf{n}, & \text{on } \Gamma_0, \\ (\nabla \times \overline{\mathbf{F}^j}) \times \mathbf{n} = 0, & \text{on } \Gamma \setminus \Gamma_0. \end{cases} \tag{3.11}$$

In the sequel, we consider synthetic data $\mathbf{E}^j_{\text{obs}}$, $1 \leq j \leq M$. This will be precised in Section 5.

4 The Adaptive Eigenspace Inversion method

In this section, we describe the reconstruction procedure used to solve $(\mathcal{P})$. It is based on the AEI method. The originality of the method comes from the parametrization space. Instead of looking for the value of the unknown coefficient κ at each node of the mesh, it is projected first in the basis of the eigenvectors of the Laplacian operator. Then, an iterative process is applied to adapt both the mesh and the basis.

4.1 Choice of the coefficient parametrization

The unknown coefficient κ_{ex} is a function of $\mathbf{x}$ in Ω. In order to numerically recover κ_{ex} in Ω, we have first to choose a discretization space. A natural choice would be to use the $\mathbb{P}^1$ Lagrange basis functions $(\psi_\ell)_{1 \leq \ell \leq N}$ with N the number of internal nodes of the mesh. In the minimization method, the approximate coefficient κ_N is decomposed under the form

$$\kappa_N(\mathbf{x}) = \kappa_b(\mathbf{x}) + \sum_{\ell=1}^{N} d^\ell \psi_\ell(\mathbf{x}), \quad \mathbf{x} \in \Omega, \tag{4.1}$$

where the function κ_b is a lifting of the boundary value of κ_{ex}, assumed to be known (and not necessarily constant), obtained as the solution of the following problem:

$$\begin{cases} -\Delta \kappa_b = 0, & \text{in } \Omega, \\ \kappa_b = \kappa_{ex}, & \text{on } \Gamma. \end{cases}$$

The unknowns in (4.1) are the complex values d^ℓ for $\ell = 1$ to N. At each node of the computational domain, there are two degrees of freedom: the real and the imaginary parts of d^ℓ. The dimension of the minimization space is thus equal to $2N$.

In our method, we propose another L^2 basis. We look for an approximation κ_L of the exact coefficient κ_{ex} in the space spanned by the L first eigenfunctions of the Laplacian operator, that is

$$\kappa_L(\mathbf{x}) = \kappa_b(\mathbf{x}) + \sum_{\ell=1}^{L} \kappa^\ell \phi_\ell(\mathbf{x}), \quad \mathbf{x} \in \Omega, \tag{4.2}$$

where ϕ_ℓ, $1 \leq \ell \leq L$, is solution to the following eigenvalue problem

$$\begin{cases} -\Delta \phi_\ell = \lambda_\ell \phi_\ell, & \text{in } \Omega, \\ \phi_\ell = 0, & \text{on } \Gamma, \end{cases} \tag{4.3}$$

with λ_ℓ the corresponding eigenvalue. One advantage of this approach is to decouple the mesh size N and the dimension of the minimization space (size $2L$ with $L \ll N$). In Section 5.2, a numerical comparison is drawn between these two parametrizations.

4.2 Adaptation of the basis

In the specific case of a discontinuous coefficient, we propose an adaptive method to improve the accuracy of the reconstruction and to capture the discontinuity lines. It consists in four steps.

Step 1: We choose a parametrization for the coefficient, either (4.1) or (4.2). We solve the minimization problem (3.2) using the BFGS algorithm. We then compute a first approximate coefficient, denoted by $\kappa_{L_1}^{(1)}$, in the initial mesh. We will give in Section 5.1 a method to find the dimension L_1 of the basis.

Step 2: The information contained in the approximation $\kappa_{L_1}^{(1)}$ is used both to adapt the mesh and to construct another basis that better represents the coefficient. The principle of the basis adaptation is the following: we look for the unknown coefficient $\kappa_{L_2}^{(2)}$ in the space spanned by the L_2 first eigenfunctions $(\phi_\ell)_{1\leq\ell\leq L_2}$ of an elliptic operator, that is

$$\begin{cases} -\nabla\cdot(A^{(2)}\nabla\phi_\ell) = \lambda_\ell\phi_\ell, & \text{in } \Omega, \\ \phi_\ell = 0, & \text{on } \Gamma, \end{cases} \tag{4.4}$$

where the matrix function is computed from the knowledge of the first iterate $\kappa_{L_1}^{(1)}$ such that

$$A^{(2)}(\mathbf{x}) = \frac{1}{\max\{|\nabla\kappa_{L_1}^{(1)}(\mathbf{x})|,\eta\}}\mathrm{Id},\ \mathbf{x}\in\Omega.$$

The matrix Id is the identity matrix. The parameter $\eta > 0$ is small such as $\eta = 10^{-3}$ and allows the denominator of $A^{(2)}(\mathbf{x})$ not to vanish. By considering this new elliptic operator, the variations of the eigenfunctions are concentrated in the regions where the coefficient $\kappa_{L_1}^{(1)}$ varies, in particular close to the discontinuities of κ_{ex} (see Figure 2). We solve the minimization problem (3.2) using the BFGS algorithm to compute $\kappa_{L_2}^{(2)}$.

Step 3: We search the coefficient $\kappa_{L_3}^{(3)}$ such that

$$\kappa_{L_3}^{(3)}(\mathbf{x}) = \kappa_b(\mathbf{x}) + \sum_{\ell=1}^{L_3}\kappa^{(3),\ell}\phi_\ell(\mathbf{x}), \quad \text{where} \quad \begin{cases} -\nabla\cdot(A^{(3)}\nabla\phi_\ell) = \lambda_\ell\phi_\ell, & \text{in } \Omega, \\ \phi_\ell = 0, & \text{on } \Gamma, \end{cases}$$

with the choice

$$A^{(3)}(\mathbf{x}) = \frac{1}{\max\{|\nabla\kappa_{L_2}^{(2)}(\mathbf{x})|^2,\eta\}}\mathrm{Id},\ \mathbf{x}\in\Omega.$$

Here again, the BFGS method is applied to solve the minimization problem.

Step 4: In the last step, we search the coefficient $\kappa_{L_4}^{(4)}$ such that

$$\kappa_{L_4}^{(4)}(\mathbf{x}) = \kappa_b(\mathbf{x}) + \sum_{\ell=1}^{L_4}\kappa^{(4),\ell}\phi_\ell(\mathbf{x}), \quad \text{where} \quad \begin{cases} -\nabla\cdot(A^{(4)}\nabla\phi_\ell) = \lambda_\ell\phi_\ell, & \text{in } \Omega, \\ \phi_\ell = 0, & \text{on } \Gamma, \end{cases}$$

and $A^{(4)}$ is chosen following an anisotropic criterion. The idea is to take into account the orientation of the discontinuity lines of κ_{ex} and to accord a preference to variations of the basis functions in the direction of its gradient. To do that, as presented in Figure 1, we take a new orthonormed system $(\mathbf{x}, X_1, X_2)$ whose first axis is locally oriented by the gradient of $\kappa_{L_3}^{(3)}$ and we define the rotation matrix P as follows:

$$P(\mathbf{x}) = \frac{1}{|\nabla\kappa_{L_3}^{(3)}(\mathbf{x})|}\begin{pmatrix} \dfrac{\partial\kappa_{L_3}^{(3)}}{\partial x_1}(\mathbf{x}) & -\dfrac{\partial\kappa_{L_3}^{(3)}}{\partial x_2}(\mathbf{x}) \\ \dfrac{\partial\kappa_{L_3}^{(3)}}{\partial x_2}(\mathbf{x}) & \dfrac{\partial\kappa_{L_3}^{(3)}}{\partial x_1}(\mathbf{x}) \end{pmatrix}.$$

In the new system, we choose to give more weight to the direction of the gradient, by setting:

$$A^{(4)}(\mathbf{x}) = \frac{1}{\max\{|\nabla \kappa^{(3)}_{L_3}(\mathbf{x})|^2, \eta\}} P(\mathbf{x}) C(\mathbf{x}) P^{-1}(\mathbf{x}),$$

with

$$C(\mathbf{x}) = \begin{pmatrix} \dfrac{1}{\max\{|\nabla \kappa^{(3)}_{L_3}(\mathbf{x})|^2, \eta\}} & 0 \\ 0 & 1 \end{pmatrix}.$$

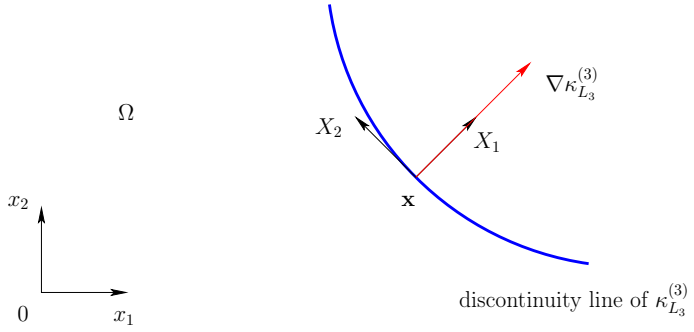

Figure 1 – Illustration of the change of coordinate system for the anisotropic case (Step 4 of the AEI method).

Notice that at each step s, we increase the power q of the norm of the gradient in the definition of the matrix $A^{(s)}$: we start from $q = 0$ at Step 1 (in that case, $A^{(1)} = \mathrm{Id}$ and the associated elliptic operator is the Laplacian) to $q = 4$ in the direction of the gradient at Step 4. This process allows to refine increasingly the reconstrution of the coefficient κ_{ex}. Furthermore, at each step, we use the solution obtained at the previous step to adapt the mesh. We consider a classical mesh adaptation algorithm. It is based on the Hessian of the solution $\kappa^{(s)}_{L_s}$, $s \in [\![1, 3]\!]$. It concentrates the nodes of the mesh where the solution varies to decrease the approximation error without increasing the computational time [16]. The accuracy of the adaptative eigenspace basis is illustrated in Figure 2. The real part of the exact coefficient is presented in Figure 15(a). For $s \in [\![1, 4]\!]$, we project the exact coefficient in the space spanned by the $L_s = 49$ first eigenfunctions of the corresponding elliptic operator. In Figure 2, we report the mesh obtained at each step, the behavior of the first and the 26th eigenfunctions, and the projection of the exact coefficient in the successive eigenspaces. The projection error in L^2-norm is efficiently decreased during the process.

5 Numerical results

In this section, we discuss the numerical solution of the inverse medium problem $(\mathcal{P})$ by using the AEI method. We reconstruct the complex refractive index κ_{ex} of the medium from synthetic noisy data. First, we describe the data set and the discretized version of the AEI method. Secondly, we perform only the Step 1 of the method to compare the coefficient parametrizations (4.1) and (4.2). Finally, we present the reconstruction of the exact coefficient κ_{ex} via the complete iterative process for different configurations.

	Step 1	Step 2	Step 3	Step 4
Mesh	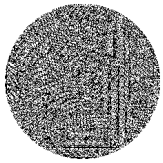	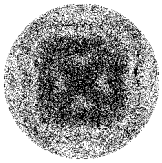	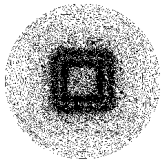	
ϕ_1	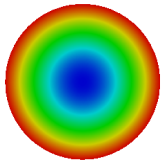	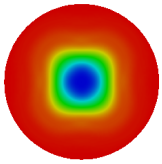	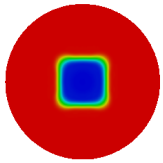	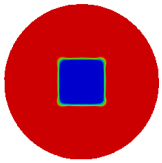
ϕ_{26}	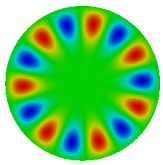	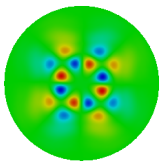	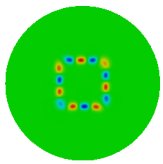	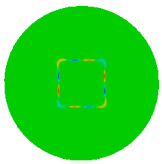
$\Re(\kappa_b + \sum_{\ell=1}^{49}(\kappa_{ex}, \phi_\ell)\phi_\ell)$	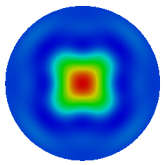	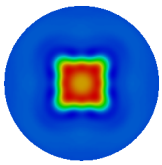	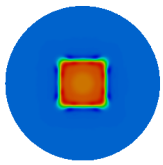	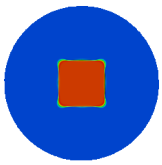
	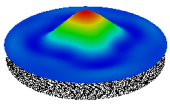	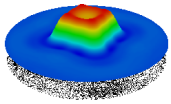	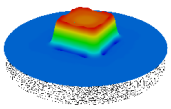	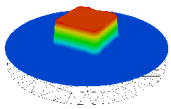
Projection error	1.30%	0.56%	0.19%	0.06%

Figure 2 – At each step: the adapted mesh, the eigenfunctions ϕ_1 and ϕ_{26}, and the projection of the exact coefficient $\Re(\kappa_{ex})$ (cf. Figure 15(a)) in the corresponding basis.

5.1 Description of data driven simulations and implementation

The domain Ω is the unit circle. The partition of the boundary is illustrated in Figure 3(a). The observations are collected on the boundary $\Gamma_0 := \{(\cos(t), \sin(t)), t \in [\gamma\pi, 2\pi]\}$ with the parameter $\gamma \in [0, 2[$. We consider full data in the case $\gamma = 0$ and limited-view ones otherwise. We look for different types of coefficients κ_{ex} :

- Continuous functions of $\mathbf{x}$.
- Piecewise constant coefficients:

$$\kappa_{ex}(\mathbf{x}) = \begin{cases} \kappa_p & \text{if } \mathbf{x} \in \omega_0, \\ \kappa_b & \text{otherwise,} \end{cases}$$

  where κ_p and κ_b are complex constants. The inhomogeneity of the medium is supported in the subdomain $\omega_0 \subsetneq \Omega$.

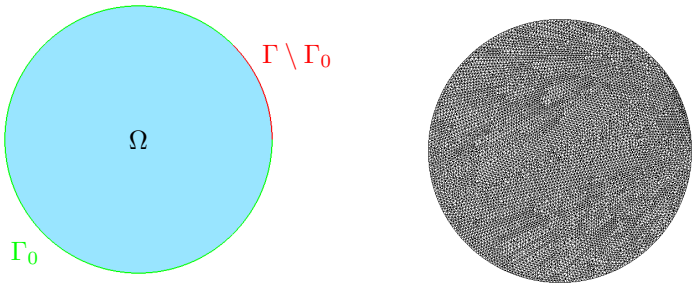

(a) Observation boundary Γ_0. (b) Triangular mesh.

Figure 3 – Computational domain.

Synthetic noisy data

We work with synthetic data. Let $1 \leq j \leq M$, $M \in \mathbb{N}^*$. We take incident plane waves

$$\mathbf{E}^j_{\text{inc}}(\mathbf{x}) = \boldsymbol{\eta}_j^{\perp} e^{ik\sqrt{\kappa_b}\boldsymbol{\eta}_j \cdot \mathbf{x}}, \tag{5.1}$$

of wave vector $\boldsymbol{\eta}_j = (\cos(2(j-1)\pi/M), \sin(2(j-1)\pi/M))^t$. The vector $\boldsymbol{\eta}_j^{\perp}$ is a unit vector orthogonal to $\boldsymbol{\eta}_j$ and κ_b a complex constant that characterizes the reference background medium. The square-root $\sqrt{\kappa_b}$ stands for the classical complex square-root with branch-cut along the negative real axis. At fixed frequency ω, recall that the wavenumber k is equal to $k = \omega\sqrt{\varepsilon_0\mu_0}$ with the permeability and the permittivity of the vacuum $\mu_0 = 4\pi\ 10^{-7} H.m^{-1}$ and $\varepsilon_0 = 8.854187\ 10^{-12} F.m^{-1}$. Examples of such waves (5.1) are illustrated in Figure 4. Incident waves are attenuated by the dissipative medium properties.
The synthetic data $\mathbf{E}^j$ are obtained by solving the forward problem (2.3)-(2.5) with the exact coefficient κ_{ex} and the boundary data $\mathbf{g}^j := (\nabla \times \mathbf{E}^j_{\text{inc}}) \times \mathbf{n}$. We consider a triangular mesh of the computational domain Ω.

We adopt Nédélec edge elements of order 1 [28] which give natural approximation spaces of $H(\text{curl}; \Omega)$. The basis functions are associated with the edges of the mesh. To avoid the *inverse crime*, we use Nédélec finite elements of different orders for the numerical solution of the direct and

the inverse problems. Furthermore, to model possible experimental errors, we can add a Gaussian noise as

$$\mathbf{E}^j_{\text{obs}}(\mathbf{x}_i) := (1 + \alpha\, rand(\mathbf{x}_i))\, \mathbf{E}^j(\mathbf{x}_i), \tag{5.2}$$

where $\mathbf{x}_i$ denotes the vertex i of a given discretization of the boundary Γ_0, *rand* gives uniformly distributed random number in $[-1, 1]$, and α is the level of noise. Note that the model of noise is a multiplicative noise and not an additive one. Our choice is motivated by [13]. The input data for the inverse problem are thus the M sets $(\mathbf{E}^j_{\text{obs}}, \mathbf{g}^j)$, $j = 1, \ldots, M$.

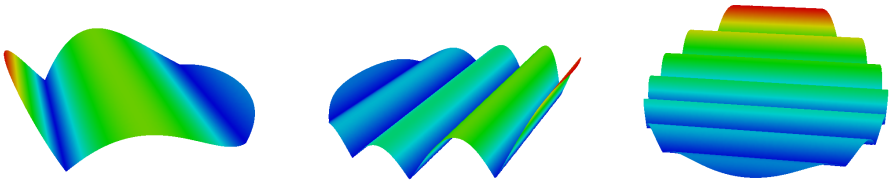

(a) $j = 7$, $\omega = 2\pi 10^8$Hz, $\kappa_b = 1 + i$

(b) $j = 13$, $\omega = 6\pi 10^8$Hz, $\kappa_b = 1 + i/3$

(c) $j = 2$, $\omega = 10\pi 10^8$Hz, $\kappa_b = 1 + 0.2i$

Figure 4 – Incident waves used to illuminate the domain.

Implementation of the reconstruction method

Let us now describe the implementation of the reconstruction method. At each step $s \in [\![1, 4]\!]$ of the adaptive process, we solve the minimization problem (3.2) iteratively by the BFGS algorithm with a tolerance of ϵ. The initial guess at Step $s = 1$ for the inverse problem is the coefficient $\kappa := \kappa_b$ that represents an a priori medium. Next, the initial guess at Step $s \in [\![2, 4]\!]$ is the approximate coefficient $\kappa^{(s-1)}$ computed at the previous step. The eigenvalue problems are solved by using the toolbox included in FreeFem++ [21]. These tools are based on the library Arpack++ which implements the "Implicit Restarted Arnoldi Method" (IRAM) combining Arnoldi factorizations with an implicitly shifted QR method [24]. For the mesh adaptation, we pay a special attention to have the more refined mesh but without increasing the total number of vertices.

The number L of eigenfunctions used in the expansion (4.2) is automatically fixed in the following way. At each step s of the AEI method, we start with $L = 1$ and we increase it from 10 to 10. We stop when adding 10 eigenfunctions to the basis does not allow to decrease significantly the value of the functional J^M. Thus, we set L_s equal to the first value L such that the following stopping criterion is met:

$$\frac{J^M(\kappa_L^{(s)}) - J^M(\kappa_{L+10}^{(s)})}{J^M(\kappa_L^{(s)})} < \delta, \tag{5.3}$$

where $\delta > 0$ can depend on the level of noise α if it is known *a priori*.

At each iteration of BFGS, the computation of the gradient (3.10) needs the solution of the forward problem (2.3)-(2.5) and the adjoint problem (3.5)-(3.6). To this end, we choose Nédélec edge elements of order 0, and not of order 1 used to generate the data. We solve the $2M$ problems in parallel thanks to MPI. Note that the unknown coefficient is not defined on the same mesh used to solve the state and adjoint problems. Table 1 gathers the numerical values used for all the following examples, unless specified otherwise where appropriate.

The complete numerical procedure for solving the inverse medium problem is the following:

ω	γ	M	α	ϵ	δ
$2\pi 10^8$ Hz	0.1	16	0	10^{-3}	10^{-3}

Table 1 – Fixed values in the remaining of the Article (unless specified otherwise).

AEI algorithm

- *At fixed frequency ω, generate the synthetic noisy data $\mathbf{E}^j_{\text{obs}}$ (5.2), $1 \le j \le M$, on the boundary $\Gamma_0 := \{(\cos(t), \sin(t)), t \in [\gamma\pi, 2\pi]\}$.*
- *AEI steps: for $s \in [\![1, 4]\!]$ (Step s, see Section 4.2)*
  - *If $s > 1$ then adapt the mesh with respect to $\kappa^{(s-1)}_{L_{s-1}}$.*
  - *Fix $L = 1$. While the stopping criterion (5.3) is not satisfied,*
    - *Apply the BFGS algorithm with a tolerance of ϵ.*

      Initialization: $\kappa^{(s)}_L = \begin{cases} \kappa_b & \text{if } s = 1, \\ \kappa^{(s-1)}_{L_{s-1}} & \text{otherwise.} \end{cases}$

      Expand the coefficient in the space spanned by the L first eigenfunctions of the elliptic operator (associated with Step s).

      At each iteration n:
      - *Solve M forward problems in parallel.*
      - *Solve M adjoint problems in parallel.*
      - *Compute the gradient (3.10) of the cost functional J^M.*
    - *Increase $L = L + 10$.*
  - *Set $L_s = L$.*
- *Output: $\kappa^{(4)}_{L_4}$.*

5.2 Coefficient parametrization: $\mathbb{P}_1$ versus eigenspace method

In this section, we numerically compare the parametrizations (4.1) and (4.2) in the configuration where the exact coefficient is defined by

$$\kappa_{ex}(\mathbf{x}) = \begin{cases} 2 + 2i & \text{if } \mathbf{x} \in \omega_0, \\ 1 + i & \text{otherwise,} \end{cases} \tag{5.4}$$

with the ellipse $\omega_0 := \{(x_1, x_2) \in \mathbb{R}^2 | (x_1 - 0.2)^2 + 0.7(x_2 + 0.1)^2 \le 0.09\}$. Dielectrical permittivity ε and electric conductivity σ are given by piecewise constant functions with the same support but different values, namely

$$\varepsilon(\mathbf{x}) = \begin{cases} 2\varepsilon_0 & \text{if } \mathbf{x} \in \omega_0, \\ \varepsilon_0 & \text{otherwise,} \end{cases} \quad \text{and } \sigma(\mathbf{x}) = \begin{cases} 2\omega\varepsilon_0 & \text{if } \mathbf{x} \in \omega_0, \\ \omega\varepsilon_0 & \text{otherwise.} \end{cases}$$

To carry out the comparison, we perform only the Step 1 of the method by varying different parameters (such as the number of observations, the boundary Γ_0 of observation, etc). The relative error in L^2-norm on the exact coefficient κ_{ex} is defined by

$$\frac{\int_\Omega |\kappa_{ex} - \kappa^{(1)}_{L_1}|^2 d\Omega}{\int_\Omega |\kappa_{ex}|^2 d\Omega},$$

where $\kappa^{(1)}_{L_1}$ is the numerical reconstructed coefficient at the end of Step 1.

Projection error

First, we compare the projection error on the coefficient κ_{ex} (5.4) using the parametrizations (4.1) and (4.2) with respect to the dimension, setting $L = N$. Results are reported on Figures 5 and 6. The two methods allow a good representation of the exact coefficient and the projection error decreases with the dimension. We obtain errors equal to 0.22% and 0.07% taking $L = N = 1688$ respectively for the $\mathbb{P}_1$ and the eigenspace basis (cf. Figure 5). Thus, the eigenspace approach provides more accurate contours of the inclusion than the $\mathbb{P}_1$ basis (cf. Figure 6).

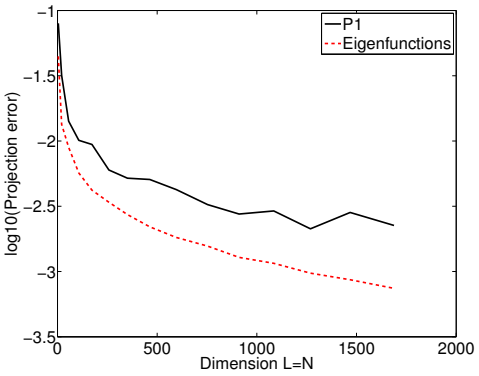

Figure 5 – Comparison of two parametrizations to represent the unknown coefficient κ_{ex}. Projection error in L^2-norm with respect to the dimension.

Convergence of the BFGS algorithm

We study the convergence of the BFGS algorithm for the minimization of the functional J^M (cf. (3.8)). We consider the same number of degrees of freedom in both parametrizations. We fix N internal mesh nodes for the classical $\mathbb{P}1$ basis and L_1 eigenvectors for the eigenspace method, with $L_1 = N = 49$. The BFGS tolerance is fixed equal to $\epsilon = 10^{-4}$. We report on Figure 7 the history of the relative norm $r := \|D_\kappa J^M(\kappa)\|_{l_2}/\|D_\kappa J^M(\kappa_b)\|_{l_2}$ in logarithm scale with respect to the number n of iterations. Here, κ is the approximate coefficient at iteration n.

The convergence is faster for the eigenspace approach than for the $\mathbb{P}_1$ basis (135 iterations against 260). The corresponding reconstructed dielectric permittivities at the end of Step 1 are presented on Figure 8 (figures at the left). Similar results are obtained also for the conductivity.

Influence of the parameter set: full or limited-view data, number of observations, level of noise.

We apply the Step 1 of the method for different configurations. We study the influence of the parameter set on the relative error between the exact and reconstructed coefficients. Results are reported in Table 2. Recall that the fixed values are given in Table 1. First, we vary the length of the boundary Γ_0 on which the observations are recorded: full-data ($\gamma = 0$, i.e. $\Gamma_0 = \Gamma$) to limited-view data ($\gamma = 1.75$, i.e. $\Gamma_0 := \{(\cos(t), \sin(t)), t \in [1.75\pi, 2\pi]\}$). As expected, errors increase with partial boundary measurements and remain under 3.29%. Then, we change the number of observations. Performance of Step 1 is not very sensitive to this parameter. The value $M = 16$ seems to be quasi-optimal for the eigenspace approach and taking M superior to 16 does not really improve accuracy. The $\mathbb{P}_1$ basis is slightly unstable with respect to this parameter. Finally, we add a Gaussian noise of level α, where α is varying between 0.005 and 0.05 (i.e. 0.5% to 5%). The

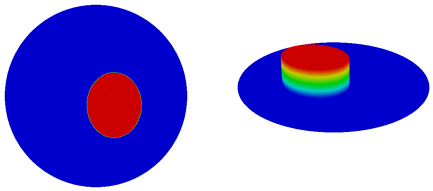

(a) Real part of the exact coefficient κ_{ex} (5.4), (center) 2D view, (right) 3D view.

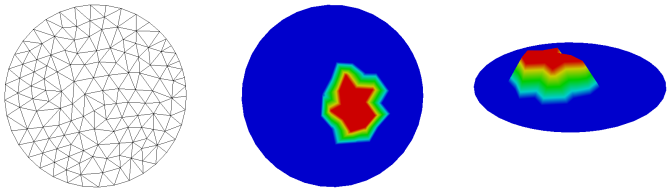

(b) Parametrization using $\mathbb{P}^1$ Lagrange finite elements: (left) a mesh with 107 interior nodes, (center) the projection of $\Re(\kappa_{ex})$ in 2D view, (right) corresponding 3D view. Relative projection error in L^2-norm = 1.0%.

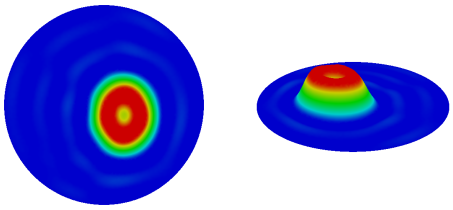

(c) Parametrization using the 107 first eigenfunctions of the Laplacian operator: (center) projection of $\Re(\kappa_{ex})$ in 2D view, (right) corresponding 3D view. Relative projection error in L^2-norm = 0.6%.

Figure 6 – Comparison of the two parametrizations to represent the coefficient κ_{ex}.

approximation of the coefficient κ_{ex} is less precise when the level of noise increases. But here again, the inclusion ω_0 is localized in each case.

γ	$\mathbb{P}_1$	Eigenspace	M	$\mathbb{P}_1$	Eigenspace	α	$\mathbb{P}_1$	Eigenspace
0	1.58%	1.39%	4	1.37%	1.55%	0.005	1.47%	1.45%
0.25	1.4%	1.69%	8	1.33%	1.43%	0.01	1.62%	1.34%
1	2%	1.98%	16	1.46%	1.39%	0.02	1.77%	1.35%
1.75	3.29%	2.97%	32	1.61%	1.38%	0.05	2.7%	2.62%

Table 2 – Relative errors in L^2 norm between the exact and reconstructed coefficients with respect to different parameters: full or limited-view data (parameter γ), the number of observations M, and the level of noise (parameter α). $N = L_1 = 49$.

Now, we test the effect of the frequency and also of the dimension of the minimization space.

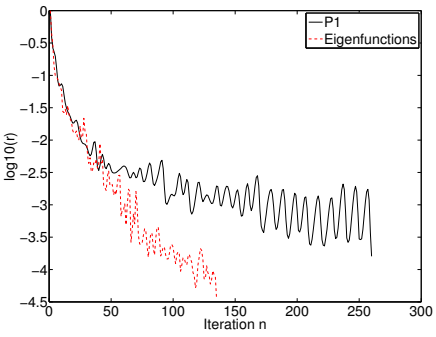

Figure 7 – Convergence of the BFGS minimization algorithm (Step 1 of the AEI method): decrease of the gradient norm.

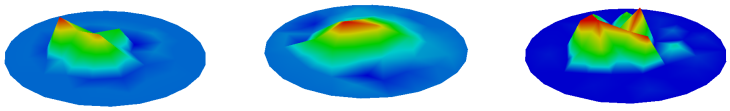

(a) $\mathbb{P}_1$ basis ($N = 49$). No noise and observations with $\gamma = 0.1$ (left). No noise and observations with $\gamma = 1.75$ (center). Level noise 5% and observations with $\gamma = 0.1$ (right).

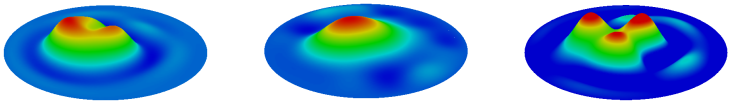

(b) Eigenspace ($L_1 = 49$). No noise and observations with $\gamma = 0.1$ (left). No noise and observations with $\gamma = 1.75$ (center). Level noise 5% and observations with $\gamma = 0.1$ (right).

Figure 8 – Reconstructed dielectric permittivities at the end of Step 1 for different set of parameters.

In the latter comparison, we fix $L_1 = N$. Errors are reported in Table 3. Whatever the frequency and the dimension are, errors are similar. They are under 2%.

ω	$\mathbb{P}_1$	Eigenspace	L_1	$\mathbb{P}_1$	Eigenspace
$18\pi 10^7$ Hz	1.3%	1.44%	49	1.46%	1.4%
$2\pi 10^8$ Hz	1.46%	1.4%	228	1.72%	1.54%
$4\pi 10^8$ Hz	1.54%	1.35%	516	1.85%	1.61%
$8\pi 10^8$ Hz	1.42%	1.64%	925	1.82%	1.78%

Table 3 – Relative errors in L^2 norm between the exact and reconstructed coefficients with respect to the frequency and to the dimension L_1 ($L_1 = N$) of the minimization space.

We can conclude that the Step 1 of the AEI method provides a first reasonable approximation of the exact coefficient κ_{ex} independently of the data set and with a slightly advantage for the eigenspace approach. In the considered example, it allows the localization of the zone where the electromagnetic coefficients vary. These approximate coefficients are very good initial guesses for the iterative process. We will see in the next section that the further steps of the AEI method perform an accurate reconstruction in both form and values.

5.3 Numerical reconstruction by the Adaptive Eigenspace Method

In this section, we present the numerical reconstruction for various configurations. The inhomogeneous medium is first described as a space continuous function. Then, we consider functions having some discontinuities, namely the case of piecewise constant functions. In all the figures except Figure 13, the color scale is the same: the color blue stands for value 1 and the color red represents value 2.

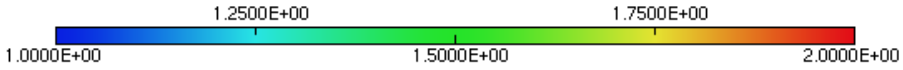

Figure 9 – Color scale for all the figures.

5.3.1 Continuous functions

We first try to recover the following exact coefficient, given as a continuous function of $\mathbf{x} = (x_1, x_2)$:

$$\kappa_{ex}(\mathbf{x}) = \frac{6 + \cos(3(x_1 + x_2)) + \cos(5x_1)}{4}. \tag{5.5}$$

Remember that in our approach we assume that the exact coefficient is known on the boundary of the domain. We can then easily compute the lifting function κ_b as the solution of the following problem:

$$\begin{cases} -\Delta\kappa_b = 0, & \text{in } \Omega, \\ \kappa_b = \kappa_{ex}, & \text{on } \Gamma. \end{cases} \tag{5.6}$$

Both functions κ_{ex} and κ_b are plotted in Figure 10, on the left and in the center respectively. In that special case where the coefficient to recover is continuous, it is useless to perform the various steps of the AEI process. Indeed, as already mentioned in Section 4.2, the AEI method allows to better capture some discontinuity lines in the coefficient and should be used in that case. Here, the first step already gives satisfactory results (see Figure 10 on the right).

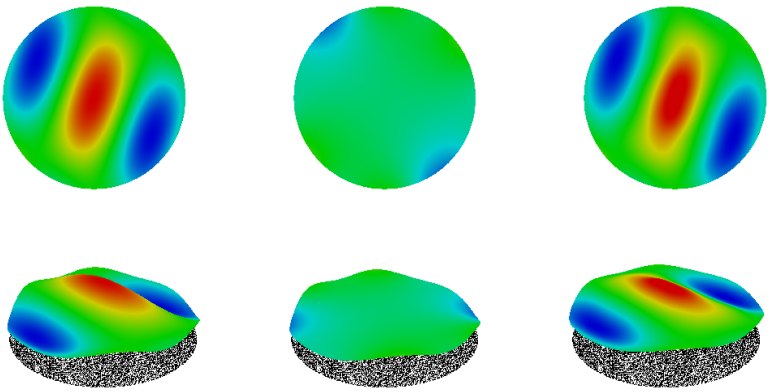

Figure 10 – Exact coefficient $\Re(\kappa_{ex})$ (left). Lifting κ_b from the known boundary value (center). Reconstructed coefficient $\Re(\kappa_{L_1}^{(1)})$ at Step 1 with $L_1 = 51$ (right).

5.3.2 Piecewise constant coefficients

A reference test-case: one ellipse.

We adopt the adaptative process to retrieve the coefficient κ_{ex} (5.4) defined in Section 5.2. We report on Figure 11 the successive reconstructed coefficients $\kappa_{L_s}^{(s)}$, $s \in [\![1, 4]\!]$. The relative L^2-error decreases at each step of the process to reach a final value equal to 0.39%. This example illustrates how each step uses information on the coefficient obtained in the previous step to improve the reconstruction. The first step of the AEI method allows to localize the perturbations in the electromagnetic coefficients, and the others to retrieve their shapes and values. For Step 1 to 4, the dimension L_s of the eigenspace is $71, 41, 51$ and 51, and the corresponding number of BFGS iterations is $100, 34, 13$ and 7. The total computational time is 5592, 1840, 831 and 578 seconds, including the iterative research of L_s. The number of vertices of each adapted mesh is around 30000. In Figure 12, we represent the results obtained at Step 4 from noisy observation data with different levels of noise according to the formula (5.2). As expected, the reconstruction error increases with the noise level but remains stable. The results are satisfactory even with 10% noise.

Small constrast.

We are interested now in determining an inhomogeneity with a small contrast, modeled by the coefficient

$$\kappa_{ex}(\mathbf{x}) = \begin{cases} 1.1 + 1.1i & \text{if } \mathbf{x} \in \omega_0, \\ 1 + i & \text{otherwise.} \end{cases} \tag{5.7}$$

We report in Figure 13 the exact (left) and the reconstructed coefficient fat Step 4 (right). For s from 1 to 4, the dimension L_s of the eigenspace is $31, 31, 21$ and 31, and the number of BFGS iterations is $29, 9, 3$ and 5 respectively. The method gives a very accurate result. This enables us to envisage applications in real biomedical situations where the discrepancy between the properties of healthy and sick tissues is small.

	Step 1	Step 2	Step 3	Step 4
Rel. L^2 error	1.61%	1.15%	0.5%	0.39%

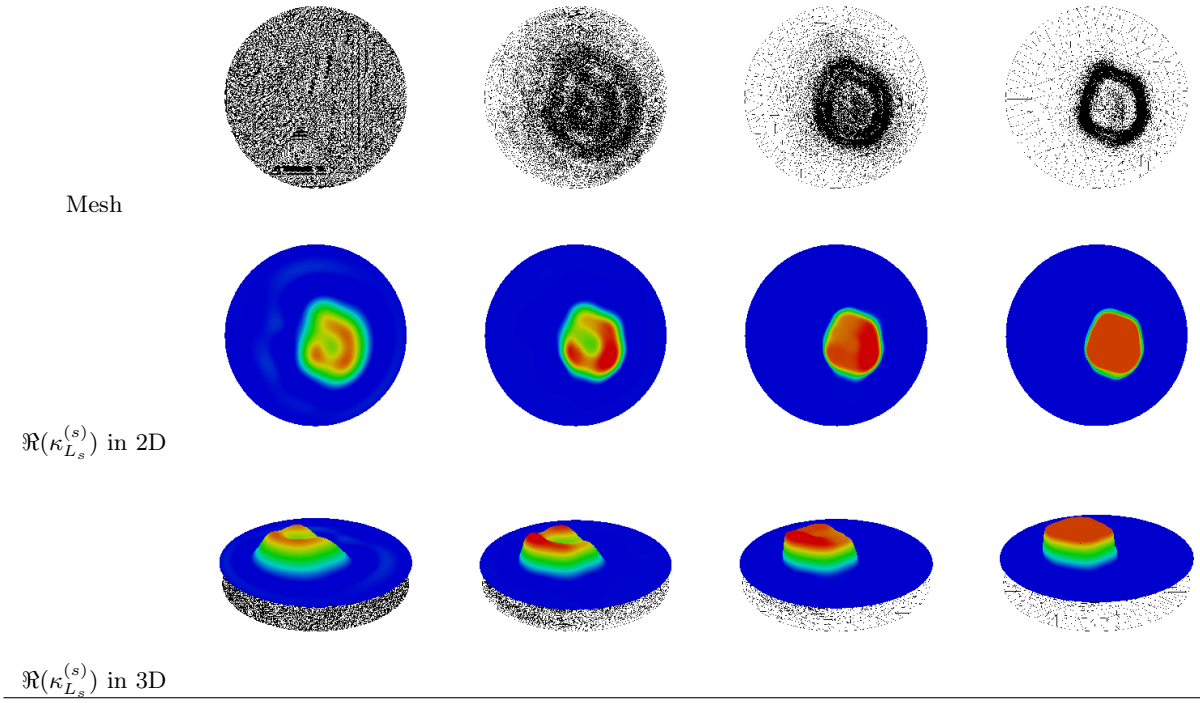

Figure 11 – The AEI method for the recovery of piecewise constant functions.

Multiple inhomogeneities.

We consider the following coefficient

$$\kappa_{ex}(\mathbf{x}) = \begin{cases} 2+2i & \text{if } \mathbf{x} \in \omega_1 \cup \omega_2, \\ 1+i & \text{otherwise.} \end{cases} \tag{5.8}$$

The inhomogeneities of the medium are represented by two ellipses $\omega_1 := \omega_0$ and $\omega_2 := \{(x_1, x_2) \in \mathbb{R}^2 | (x_1+0.5)^2 + 0.4(x_2-0.2)^2 \leq (0.15)^2\}$ of different size. The final reconstructed coefficient is given in Figure 14. For steps $s \in [\![1, 4]\!]$, the dimension L_s of the eigenspace is $71, 51, 61$ and 11, and the number of BFGS iterations is $113, 40, 16$ and 17 respectively. The relative reconstruction error at the last step is 0.93%. The AEI method performs very well the separation and the reconstruction of multiple inhomogeneities, even when their sizes and the distance between them are smaller than the wavelength. Indeed, in that case for example, the incident wavelength is $\lambda = k/2\pi = 3$ whereas the diameter of the domain Ω is only 2.

Square and star.

We further test the reconstruction of inhomogeneities with irregular contour, namely

$$\kappa_{ex}(\mathbf{x}) = \begin{cases} 2+2i & \text{if } \mathbf{x} \in \omega, \\ 1+i & \text{otherwise,} \end{cases} \tag{5.9}$$

where the subdomain ω is a square centered at the origin of side 0.4, or a star delimited by the curve $t \mapsto (0.1 + c(t)\cos(t), 0.1 + c(t)\sin(t)$, with $c(t) = (20 + 3\sin(5t) - 2\sin(15t) + \sin(25t))/50$.

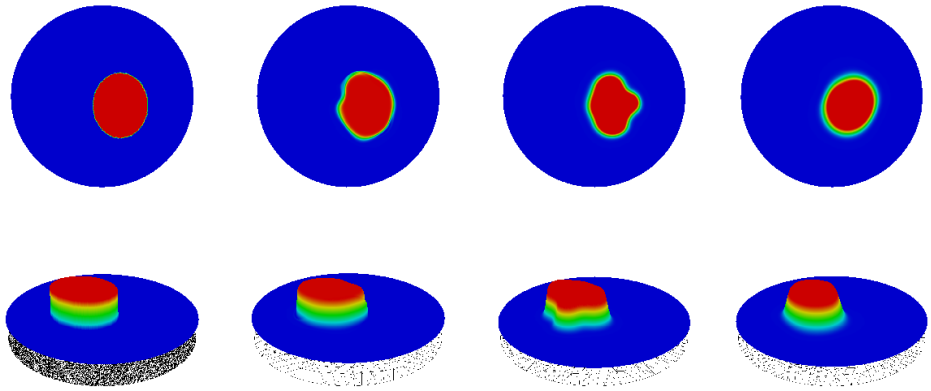

(a) (b) error = 0.34% (c) error = 0.55% (d) error = 1.99%

Figure 12 – Reconstruction of an ellipse by using the AEI method: (a) Exact coefficient $\Re(\kappa_{ex})$. (b) Reconstructed permittivity $\Re(\kappa_{L_4}^{(4)})$ with 2%-noisy data and $\delta = 5.10^{-3}$. (c) Reconstructed permittivity $\Re(\kappa_{L_4}^{(4)})$ with 5%-noisy data and $\delta = 1.10^{-2}$. (d) Reconstructed permittivity $\Re(\kappa_{L_4}^{(4)})$ with 10%-noisy data and $\delta = 5.10^{-2}$.

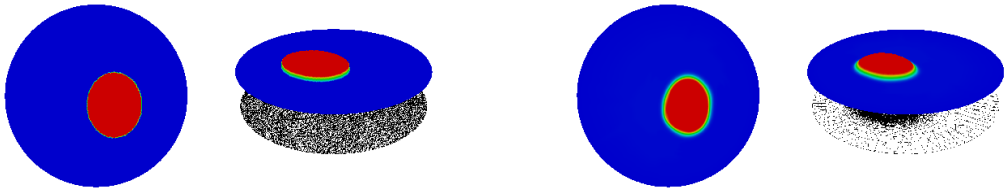

(a) Exact coefficient $\Re(\kappa_{ex})$ (b) Reconstructed permittivity $\Re(\kappa_{L_4}^{(4)})$

Figure 13 – Reconstruction of a flat ellipse by using the AEI method.

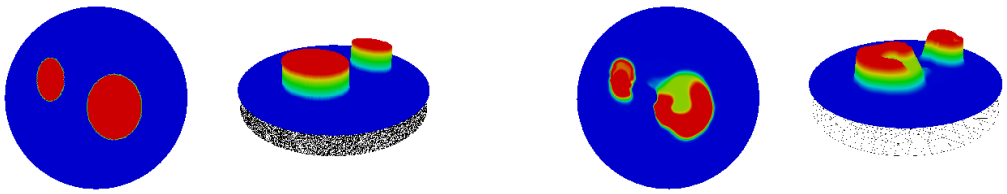

(a) Exact coefficient $\Re(\kappa_{ex})$ (b) Reconstructed permittivity $\Re(\kappa_{L_4}^{(4)})$

Figure 14 – Reconstruction of two ellipses by using the AEI method.

The AEI method still gives accurate results. The relative reconstruction error on the coefficient at the last step is 0.48% in the case of the square, and 1.03% for the star. As a comparison to highlight the efficiency of the AEI process, we have reported the reconstructed coefficients at the

Steps 1 and 4 (cf. Figures 15 and 16).

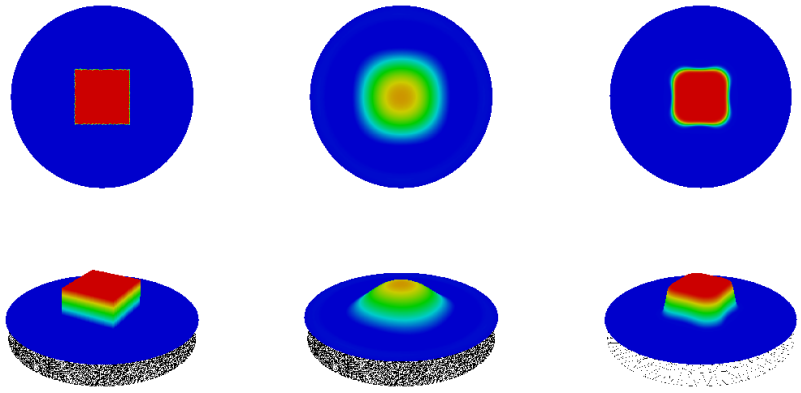

(a) (b) (c)

Figure 15 – Reconstruction of a square by using the AEI method. (a) Exact coefficient $\Re(\kappa_{ex})$. (b) Reconstructed permittivity $\Re(\kappa_{L_1}^{(1)})$ at Step 1. (c) Reconstructed permittivity $\Re(\kappa_{L_4}^{(4)})$ at Step 4.

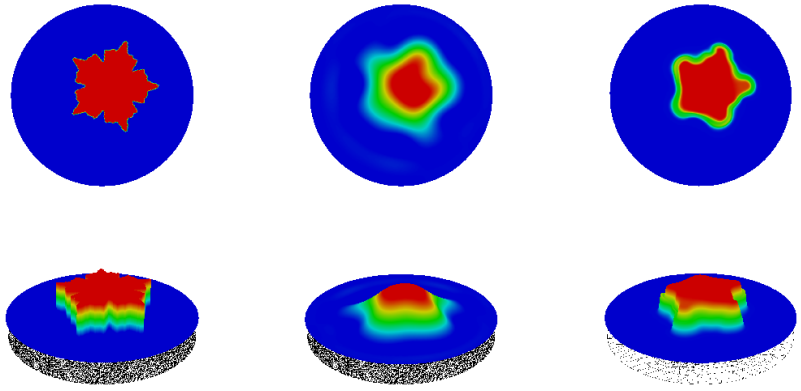

(a) (b) (c)

Figure 16 – Reconstruction of a star by using the AEI method. (a) Exact coefficient $\Re(\kappa_{ex})$. (b) Reconstructed permittivity $\Re(\kappa_{L_1}^{(1)})$ at Step 1. (c) Reconstructed permittivity $\Re(\kappa_{L_4}^{(4)})$ at Step 4.

Different dielectric permittivity and electrical conductivity.

The exact coefficient is given by

$$\kappa_{ex}(\mathbf{x}) = \begin{cases} 2\mathbb{1}_{\omega_1}(\mathbf{x}) + 2i\mathbb{1}_{\omega_2}(\mathbf{x}) & \text{if } \mathbf{x} \in \omega_1 \cup \omega_2, \\ 1+i & \text{otherwise.} \end{cases} \tag{5.10}$$

The inhomogeneity in the dielectric permittivity ε (resp. in the conductivityσ) is represented by the ellipse $\omega_1 := \omega_0$ (resp. the ellipse $\omega_2 := \{(x_1, x_2) \in \mathbb{R}^2 | (x_1 + 0.5)^2 + 0.4(x_2 - 0.2)^2 \leq (0.15)^2\}$). Notice that the inhomogeneity ω_2 is both small and close to the boundary. The final reconstructed coefficient is given in Figure 17. For steps $s \in [\![1, 4]\!]$, the dimension L_s of the eigenspace is $71, 41, 61$ and 11, and the number of BFGS iterations is $97, 34, 21$ and 8 respectively. The relative reconstruction error on the permittivity and the conductivity at the last step are 1.05% and 0.81% respectively.

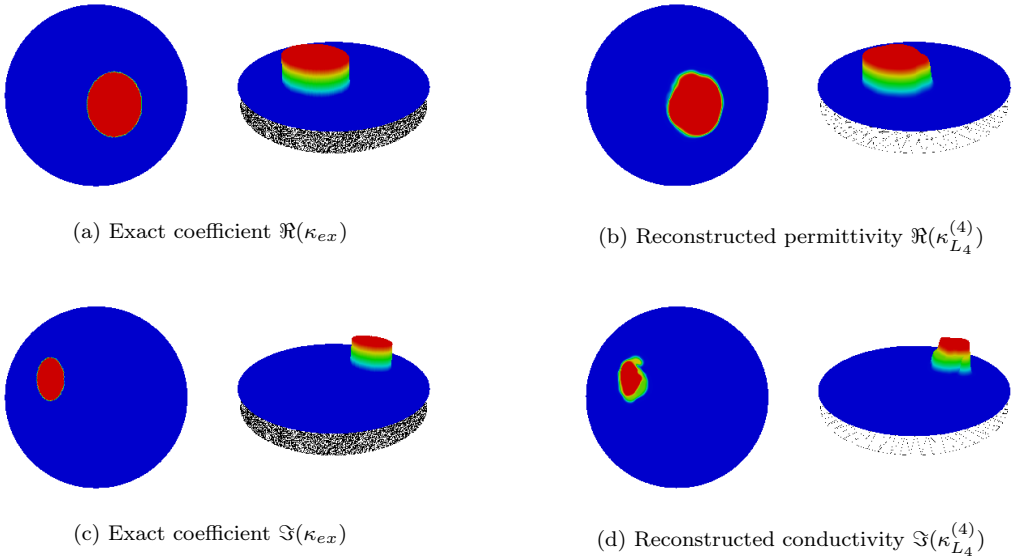

(a) Exact coefficient $\Re(\kappa_{ex})$

(b) Reconstructed permittivity $\Re(\kappa_{L_4}^{(4)})$

(c) Exact coefficient $\Im(\kappa_{ex})$

(d) Reconstructed conductivity $\Im(\kappa_{L_4}^{(4)})$

Figure 17 – Different dielectric permittivity and electrical conductivity: numerical reconstruction using the AEI method.

6 Concluding remarks and prospects

We have considered the problem of determining some of the electromagnetic properties (dielectric permittivity and electrical conductivity) of a medium in a two-dimensional bounded domain from boundary measurements at a fixed frequency. We have formulated this inverse problem as a minimization problem where the functional to be minimized measures the difference between the measured and predicted electric fields. The electromagnetic wave propagation is governed by the time-harmonic Maxwell equations.

We have presented a reconstruction procedure, called Adaptive Eigenspace Inversion (AEI) method, to solve this problem efficiently. A standard gradient-based quasi-Newton algorithm is applied to deal with the minimization problem. The originality and specificity of our approach are based on the discrete representation of the unknown complex coefficient (i.e. the refractive index of the medium). The basis composed by eigenvectors of the Laplacian operator is preferred to the more classical choice of $\mathbb{P}_1$ functions. Then, during the minimization process, both the mesh and the basis are iteratively adapted. A method is proposed to compute the dimension of the successive eigenspaces automatically, which is generally very small compared to the mesh dimension. The AEI method is able to characterize simultaneously the dielectric permittivity (real part of the coefficient) and the electrical conductivity (imaginary part of the coefficient) of a medium from partial boundary measurements of electric fields. Its performance is illustrated in several examples,

and in particular in the case of discontinuous functions. An attractive feature of the method is to yield accurate reconstructions both qualitatively and quantitatively even from noisy data.

This work has been motivated by biomedical applications, and in particular by the microwave imaging of cerebrovascular accidents [30, 31]. Strokes are characterized by dielectric properties which are slightly altered ($\pm 10\%$) from that of a healthy brain. The AEI algorithm allows to capture small perturbations in the electromagnetic coefficients (see Fig. 13) and should be a promising method to detect strokes. It has to be extended to the three-dimensional case to deal with this application.

Acknowledgements

The authors would like to thank Frédéric Nataf and Pierre-Henri Tournier for fruitful conversations. This work has been supported by the french Agence Nationale de la Recherche through project MEDIMAX, ANR-13-MONU-0012. The numerical results presented here were obtained using the ressources of the MeCS platform of the Université de Picardie Jules Verne and the authors thank Serge Van Criekingen for his help.

References

[1] H. Ammari, E. Iakovleva, D. Lesselier, G. Perrusson, *MUSIC-type electromagnetic imaging of a collection of small three-dimensional inclusions*, SIAM Journal on Scientific Computing **29** (2007), pp. 674–709.

[2] H. Ammari, H. Kang, Reconstruction of Small Inhomogeneities from Boundary Measurements, Lecture Notes in Mathematics, Volume 1846, Springer-Verlag, Berlin 2004.

[3] H. Ammari, M.S. Vogelius, D. Volkov, *Asymptotic formulas for perturbations in the electromagnetic fields due to the presence of inhomogeneities of small diameter. II. The full Maxwell equations*, J. Math. Pures Appl. **80**(8) (2001), pp. 769–814.

[4] M. Asch, S. Mefire, *Numerical localizations of 3D imperfections from an asymptotic formula for perturbations in the electric fields*, Journal of Computational Mathematics **26** No.2 (2008), pp. 149–195.

[5] G. Bao, P. Li, *Numerical solution of an inverse medium scattering problem for Maxwell's Equations at fixed frequency*, J. of Comp. Phys. **228** (2009), pp. 4638–4648.

[6] C. Bardos, G. Lebeau, J. Rauch, *Sharp sufficient conditions for the observation, control and stabilization of waves from the boundary*, SIAM J. Control Optim., **30** (1992), pp.1024–1065.

[7] L. Beilina, *Adaptive finite element method for a coefficient inverse problem for Maxwell's system*, Appl. Anal. **90** (2011), pp. 1461–1479.

[8] L. Beilina, S. Hosseinzadegan, *An adaptive finite element method in reconstruction of coefficients in Maxwell's equations from limited observations*, Applications of Mathematics, **61** (3) (2016), pp. 253–286.

[9] M. de Buhan, A. Osses, *Logarithmic stability in determination of a 3D viscoelastic coefficient and a numerical example*, Inverse Problems, 26, Number 9, pp. 95006-95043, 2010.

[10] M. de Buhan, M. Kray, *A new approach to solve the inverse scattering problem for waves: combining the TRAC and the Adaptive Inversion methods*, Inverse Problems, 29, 085009, 2013.

[11] A.P. Calderón, *On an inverse boundary value problem*, Seminar on Numerical Analysis and its Applications to Continuum Physics, Soc. Brasileira de Matemática, Rio de Janeiro, 1980.

[12] P. Caro, P. Ola, M. Salo, *Inverse boundary value problem for Maxwell equations with local data*, Comm. PDE **34** (2009), pp. 1425–1464.

[13] D. Colton, J. Coyle, P. Monk, *Recent developments in inverse acoustic scattering theory*, SIAM Review, 42, pp. 369–414, 2000.

[14] D.L. Colton, R. Kress, *Inverse Acoustic and Electromagnetic Scattering Theory*, Berlin Springer, 1998.

[15] M. Darbas, S. Lohrengel, *Numerical reconstruction of small perturbations in the electromagnetic coefficients of a dielectric material*, J. of Comp. Math. **32**(1) (2014), pp. 21–38.

[16] P.J. Frey, P.L. George, *Mesh Generation. Application to finite elements*, Wiley, London, 2008 (2nd ed.).

[17] C. Gabriel, S. Gabriel, E. Corthout, *The dielectric properties of biological tissues: I. Literature survey*, Phys. Med. Biol. 41 (1996) pp. 2231–2249.

[18] M. Grote, U. Nahum, *Adaptive Eigenspace Inversion for the Helmholtz Equation*, Proc. of the 12th International Conf. on Math. and Numerical Aspects of Wave Propagation, KIT, Karlsruhe 2015, pp. 178–179.

[19] M. Grote, M. Kray, U. Nahum, *Adaptive Eigenspace Inversion for the Helmholtz Equation*, preprint, 2016.

[20] H. Haddar, P. Monk, *The linear sampling method for solving the electromagnetic inverse medium problem*, Inverse Problems **18** (2002), pp. 891–906.

[21] F. Hecht, *New development in FreeFem++*, J. Numer. Math. **20** (3-4), (2012), pp. 251–265.

[22] T. Hohage, *Fast numerical solution of the electromagnetic medium scattering problem and applications to the inverse problem*, Journal of Computational Physics **214** (2006), pp. 224–238.

[23] C.E. Kenig, M. Salo, G. Uhlmann, *Inverse problems for the anisotropic Maxwell equations*, Duke Math. J., **157** (2011), pp. 369–419.

[24] R.B. Lehoucq, D.C. Sorensen, C. Yang *ARPACK Users'Guide: Solution of Large-Scale Eigenvalue Problems with Implicitly Restarted Arnoldi Methods*, SIAM, ISBN 0-89871-407-9, http://www.caam.rice.edu/software/ARPACK/

[25] P. Ola, L. Päivärinta, E. Somersalo, *An inverse boundary value problem in electrodynamics*, Duke Math. J. **70** (1993), pp. 617–653.

[26] P. Monk, Finite Element Methods for Maxwell's Equations, Oxford University Press, New York, 2003.

[27] A. Mordecai, *Nonlinear Programming : Analysis and Methods*, Dover Publishing, 2003.

[28] J.-C. Nédélec, *Mixed finite elements in* $\mathbb{R}^3$, Numer. Math., **35** (1980), pp. 315–341.

[29] V.G. Romanov, S.I. Kabanikhin, *Inverse problems for Maxwell's equations*, Inverse and Ill-Posed Problems Series 2, Utrecht : VSP, 1994.

[30] P.-H. Tournier, I. Aliferis, M. Bonazzoli, M. de Buhan, M. Darbas, V. Dolean, F. Hecht, P. Jolivet, I. El Kanfoud, C. Migliaccio, F. Nataf, C. Pichot, *Microwave Imaging of Cerebrovascular Accidents by Using High-Performance Computing*, hal-01356092, 2016.

[31] P.H. Tournier, M. Bonazzoli, V. Dolean, F. Rapetti, F. Hecht, F. Nataf, I. Aliferis, I. El Kanfoud, C. Migliaccio, M. de Buhan, M. Darbas, S. Semenov, C. Pichot, *Numerical Modeling and High Speed Parallel Computing: New Perspectives for Tomographic Microwave Imaging for Brain Stroke Detection and Monitoring*, hal-01343687, 2016.